ACS APPLIED MATERIALS & INTERFACES

Research Article

www.acsami.org

Contributions of CF and CF_2 Species to Fluorocarbon Film Composition and Properties for C_xF_y Plasma-Enhanced Chemical Vapor Deposition

Michael F. Cuddy and Ellen R. Fisher*

Department of Chemistry, Colorado State University, Fort Collins, Colorado 80523-1872, United States

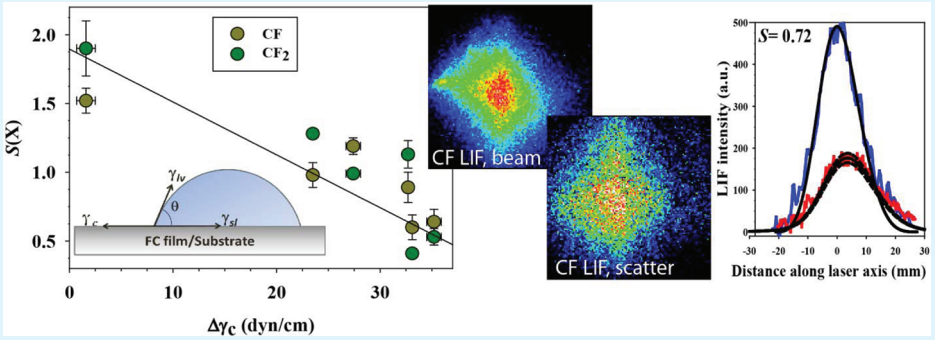

ABSTRACT: Inductively-coupled C_xF_y (y/x = 2.0−4.0) plasma systems were investigated to determine relationships between precursor chemistry, CF_n radical-surface reactivities, and surface properties of deposited films. The contributions of CF_n (n = 1, 2) radicals to film properties were probed via gas-phase diagnostics and the imaging of radicals interacting with surfaces (IRIS) technique. Time-resolved radical emission data elucidate CF(g) and CF_2(g) production kinetics from the C_xF_y source gases and demonstrate that CF_4 plasmas inherently lag in efficacy of film formation when compared to C_2F_6, C_3F_8, and C_3F_6 systems. IRIS data show that as the precursor y/x ratio decreases, the propensity for CF_n scatter concomitantly declines. Analyses of the composition and characteristics of fluorocarbon films deposited on Si wafers demonstrate that surface energies of the films decrease markedly with increasing film fluorine content. In turn, increased surface energies correspond with significant decreases in the observed scatter coefficients for both CF and CF_2. These data improve our molecular-level understanding of CF_n contributions to fluorocarbon film deposition, which promises advancements in the ability to tailor FC films to specific applications.

KEYWORDS: *plasma materials processing, surface energy, fluorocarbon polymers, radical surface interactions*

INTRODUCTION

Fluorocarbon (FC) plasmas are widely used to deposit high-quality fluorocarbon films for a range of applications including superhydrophobicity, protective coatings, and biocompatible materials. Specific applications include preparation of ultralow-k materials,[1,2] development of superhydrophobic surfaces[3] and implementation in medical devices such as stents to improve biocompatibility without initiating coagulation.[4−8] Moreover, FC polymers are increasingly utilized in micromachining to alleviate detrimental adhesion in microstructures.[9,10] The utility of fluorocarbons employed in plasma-enhanced chemical vapor deposition (PECVD) is influenced by associated parameters, including applied power (P) and system pressure (p).[11] Another driving force that dictates the efficacy and nature of FC film deposition is the choice of plasma precursor. Generally, for C_xF_y systems with low y/x ratios film deposition is most efficacious.[12] Although much evidence exists that lower y/x ratio precursors deposit FC films more readily than do high ratio feeds, the precise route toward film deposition (i.e., the phenomena which occur at the gas−surface interface) is poorly understood. The unique approach we employ attempts to correlate plasma gas-phase diagnostics with plasma-surface interface data to elucidate those processes responsible for FC film characteristics in CF_4, C_2F_6, C_3F_8, and C_3F_6 systems (y/x ranging from 2.0 to 4.0).

Gas-phase neutral species, especially of the form CF_n, have long been identified with critical functions contributing to FC film deposition.[13,14] Previous work in our group has implicated CF_2 radicals in particular for their role in film formation, as these species are readily produced at the surface of depositing FC films.[3,15,16] Here, we employed time-resolved optical emission spectroscopy (TR-OES) to investigate the initial production of CF_n species through direct decomposition of the C_xF_y precursor. An understanding of the production of film-initiating and film-propagating species in the gas-phase is of critical importance to determining the efficacy of FC film deposition. In addition, through our imaging of radicals interacting with surfaces (IRIS) experiments, we have garnered

Received: December 29, 2011
Accepted: February 24, 2012
Published: February 24, 2012

   dx.doi.org/10.1021/am2018546 | ACS Appl. Mater. Interfaces 2012, 4, 1733−1741

Table 1. IRIS Parameters Used for CF and CF_2 Surface Reactivity Measurements

						ICCD parameters	
radical	transition	fluorescent lifetime (ns)	on- resonance λ (nm)	off- resonance λ (nm)	laser dye	gate width (ns)	gate delay (μs)
CF	$A^2\Sigma^+ — X^2\Pi$	26	223.838	laser off	Coumarin 450	60	1.55
CF_2	$A^1B_1 — X^1A_1$	60	234.278	235.000	Coumarin 460	100	1.55

new insight into the behavior of these radical species near Si surfaces during substrate processing. The IRIS technique provides a spatially-resolved, two-dimensional, in situ representation of radical-substrate interactions during plasma processing. Via IRIS, we have studied the near-surface phenomena associated with CF_n radicals produced from a range of C_xF_y precursors. Coupled with gas-phase diagnostics and surface analyses, we have generated a correlation between choice of precursor, the role of gas-phase species and the net effect of FC film deposition.

A principal application of this understanding lies in tailoring the surface properties of plasma-deposited films. Important materials properties issues with respect to the specific applications include (1) surface composition; (2) surface energy; and (3) mechanical properties (e.g. cross-analyses of deposited FC films to provide compositional data). Although C_xF_y systems commonly deposit highly cross-linked films, we have achieved high $-CF_2-$ content films with low crosslinking and brittleness from hexafluoropropylene oxide and C_3F_8 by careful adjustment of plasma parameters.[17,18] In addition to chemical composition, the surface energy of a deposited film is an important metric for determining the wettability and adhesive properties of the material.[19,20] To this extent, we used a somewhat indirect route to estimate surface energies, the Zisman method,[21] that involves a straightforward empirical analysis of liquid contact angles to calculate the critical surface tension of a material. This value is in turn analogous to the surface energy of the material. The relationships determined here between film composition and physical properties with IRIS data and gas-phase diagnostics provide the basis for molecular-level film deposition mechanisms in C_xF_y plasmas.

EXPERIMENTAL DETAILS

All FC plasmas were generated in a glass tubular reactor, described at length previously,[18,22−24] by supplying 13.56 MHz rf power (P) through a Ni-plated copper coil, with P ranging from 50-150 W. C_xF_y feed gases in y/x ratios of 4 (CF_4), 3 (C_2F_6), 2.67 (C_3F_8), and 2 (C_3F_6) were individually employed (all Airgas, >95%), using 50 mTorr above base pressure for each gas. Resulting mass flows under these conditions ranged from 4.0 to 6.0 sccm.

Time-resolved optical emission spectra (TR-OES) were collected for the C_xF_y plasma systems with an Avantes AvaSpec-2048-USB2 spectrometer, blazed in the UV with a 200-450 nm wavelength range and 0.1 nm FWHM resolution. A fused quartz window on the reactor allowed for coaxial light collection from emitting plasma species via a 600 μm diameter fiber optic cable imaged onto a 10 μm slit. A nominal temporal resolution of 5 μs was realized with rapid integration times of ~3 μs under all plasma operating conditions. TR-OES measurements monitored CF* and CF_2* production from C_xF_y precursors by analyzing signals arising at 202.4 and 251.9 nm,[25,26] respectively.

The IRIS technique was used to measure scatter coefficients for CF and CF_2 radicals in a manner described in detail elsewhere.[22] Briefly, an effusive plasma molecular beam was generated from a specific C_xF_y precursor, containing essentially all relevant plasma species, and was directed through a high-vacuum ($<5 \times 10^{-6}$ Torr) interaction chamber through a series of collimating slits. This beam was intersected at a 45° angle with tunable laser light from a XeCl excimer-pumped dye laser, operating at resonance wavelengths corresponding to CF or CF_2 to induce fluorescence in the species of interest. LIF images (512 × 512 pixels with 4 x 4 pixel binning) were collected via a gated intensified charge-coupled device (ICCD) situated directly above the laser and molecular beam intersection region. Subsequently, a Si wafer on a movable substrate arm was rotated into the path of the plasma molecular beam, and a second ICCD image was obtained containing LIF signals both for the radical species being probed in the molecular beam and any species scattered from the substrate. Image subtraction yielded representative scatter profiles for the CF or CF_2 radicals. Corresponding "beam-only" and "scatter" images were cross-sectioned along the laser propagation axis using a 20 pixel average around the center of most intense fluorescence. These cross sections were compared to a geometrical model used to calculate scatter coefficients (S) for the CF and CF_2 radicals.[22] A concise list of the parameters used for determination of S(CF) and $S(CF_2)$ are provided in Table 1. All background subtractions were accomplished using images collected at off-resonant wavelengths or with the laser turned off.

XPS spectra of post-processed IRIS substrates (Si wafers) were collected using a Physical Electronics PHI-5800 ESCA/AES instrument. Typical plasma exposure times for Si wafers in the IRIS chamber were 60 to 90 minutes. XPS spectra were acquired within a day of performing depositions in the IRIS experiment. High-resolution C_{1s} and F_{1s} spectra were collected using a monochromatic Al Kα source with a pass energy of 23.5 eV. Peaks were generally shifted to the F−C binding environment at 689.0 eV. Spectral signals were deconstructed in the open-source fitting routine, XPSpeak v4.1. All fits were made by constraining the FWHM to ≤2.0 eV and using a 100% Gaussian function.

Additional FC film characterization was performed via contact angle goniometry using a Krüss DSA 10 equipped with video capture. The static contact angle (CA) of sessile water/methanol droplets of discrete compositions (Table 2) were acquired by capturing an image within 2 s of dispensing a 2 μL droplet on the FC film. CA values were measured in triplicate for each film investigated and analyzed using the circle-fitting profile. For comparisons to bare wafers, complementary experiments were performed prior to FC film deposition on the (100) face of Si containing a native oxide layer.

Table 2. Literature Liquid−Vapor Surface Tensions in Atmosphere at 25 °C[a]

constituents	γ_{lv} (dyn/cm)
100% H_2O	72.01
10/90 CH_3OH/H_2O (w/w)	56.18
20/80 CH_3OH/H_2O (w/w)	47.21
50/50 CH_3OH/H_2O (w/w)	32.86
100% CH_3OH	22.51

[a]Maximum errors <0.4%. Values taken from ref 40.

RESULTS

Representative raw OES spectra are depicted in Figure 1a for emission collected from a C_3F_8 plasma with P = 150 W, at t = 0, 0.01, and 0.20 s after plasma ignition. The plots show a conspicuous increase in emission intensity from CF_2 $A^1B_1 \rightarrow X^1A_1$ in the range of 250-400 nm, corresponding to the time dependence of the species production. Less prominently, CF emission lines from the $B^2\Delta \rightarrow X^2\Pi$ transition around 200 nm also increase in intensity as t increases to 0.20 s. The absolute

dx.doi.org/10.1021/am2018546 | ACS Appl. Mater. Interfaces 2012, 4, 1733−1741

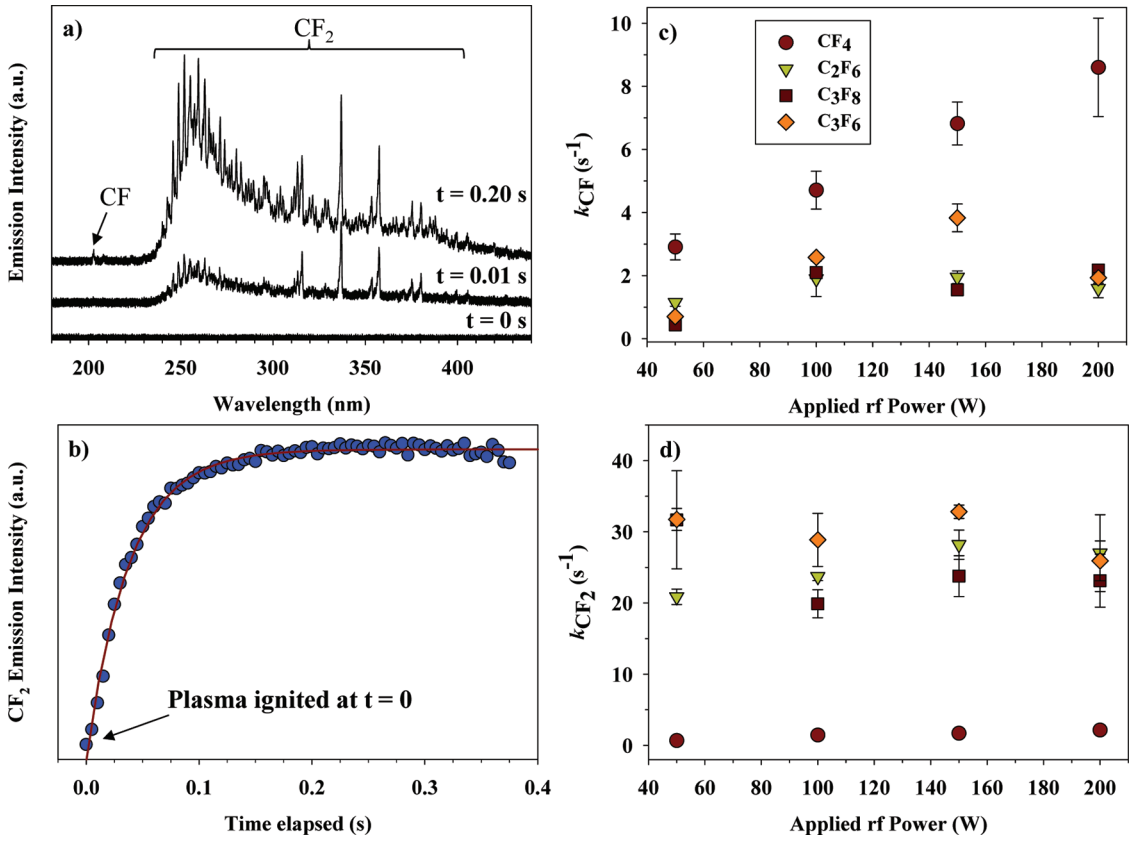

Figure 1. (a) Raw OES spectra collected at t = 0, 0.01, and 0.20 s after C_3F_8 (P = 150 W) plasma ignition. (b) CF_2 emission intensity (λ = 251.9 nm) as a function of time from plasma ignition in a P = 150 W C_3F_8 plasma. The exponential fit to these data yields a formation rate constant, $k(CF_2)$ = 26.3 s^{-1}, with $R^2 > 0.99$. (c, d) Rate constants for formation of CF and CF_2 in C_xF_y plasmas obtained from time-resolved analyses of the λ = 202.4 and 251.9 nm OES lines are plotted as functions of P, respectively.

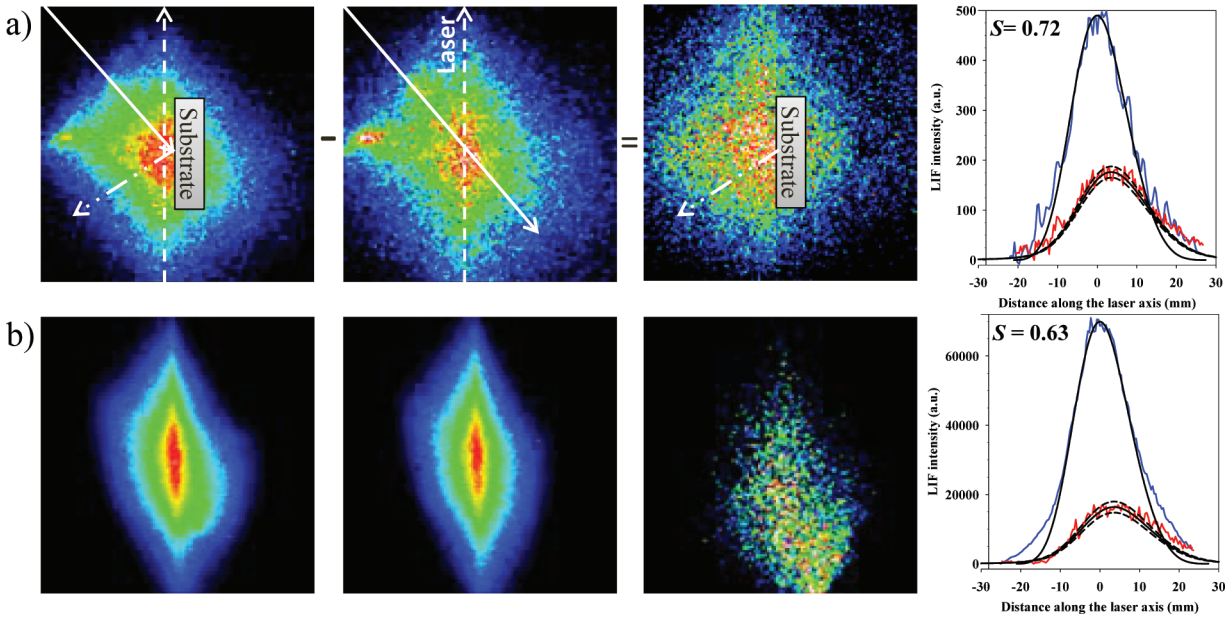

Figure 2. IRIS images for Si substrate interactions of (a) CF, and (b) CF_2, in C_3F_6 plasma molecular beams at P = 150 W. The left-most images in each set of images were acquired with a substrate rotated into the path of the plasma molecular beam (solid arrow), and thus contain signal from molecules both in the incident beam and scattered (dashed/dotted arrow). The middle panels depict signal arising solely from the plasma molecular beam. The right-most panels are obtained through image subtraction of the previous two images, resulting in a signal that corresponds to scattered molecules alone. Cross-sections along the axis of laser propagation are compared to geometric simulations to obtain a scatter coefficient, S, where $S(CF)$ = 0.72 and $S(CF_2)$ = 0.63 for a and b, respectively.

dx.doi.org/10.1021/am2018546 | ACS Appl. Mater. Interfaces 2012, 4, 1733–1741

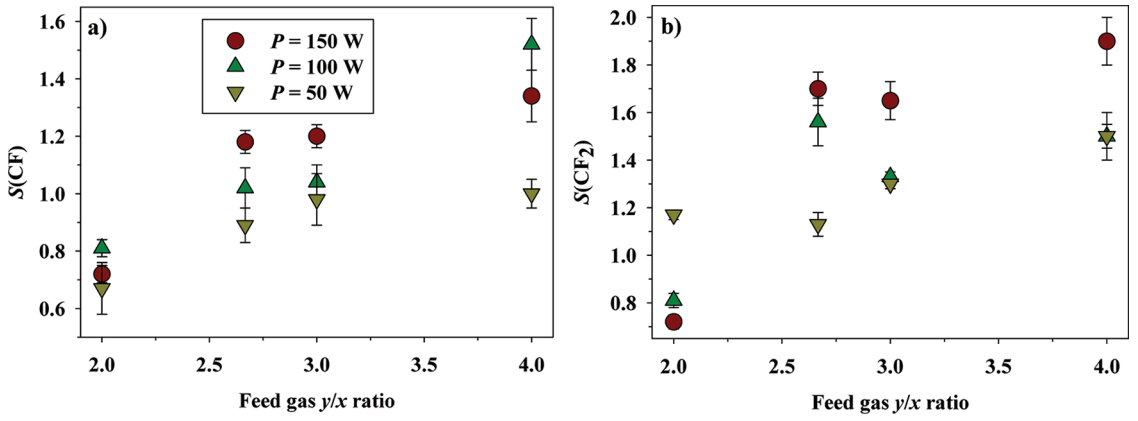

Figure 3. Scatter coefficients for (a) CF and (b) CF_2 as a function of C_xF_y feed gas y/x ratio at P = 50, 100, and 150 W.

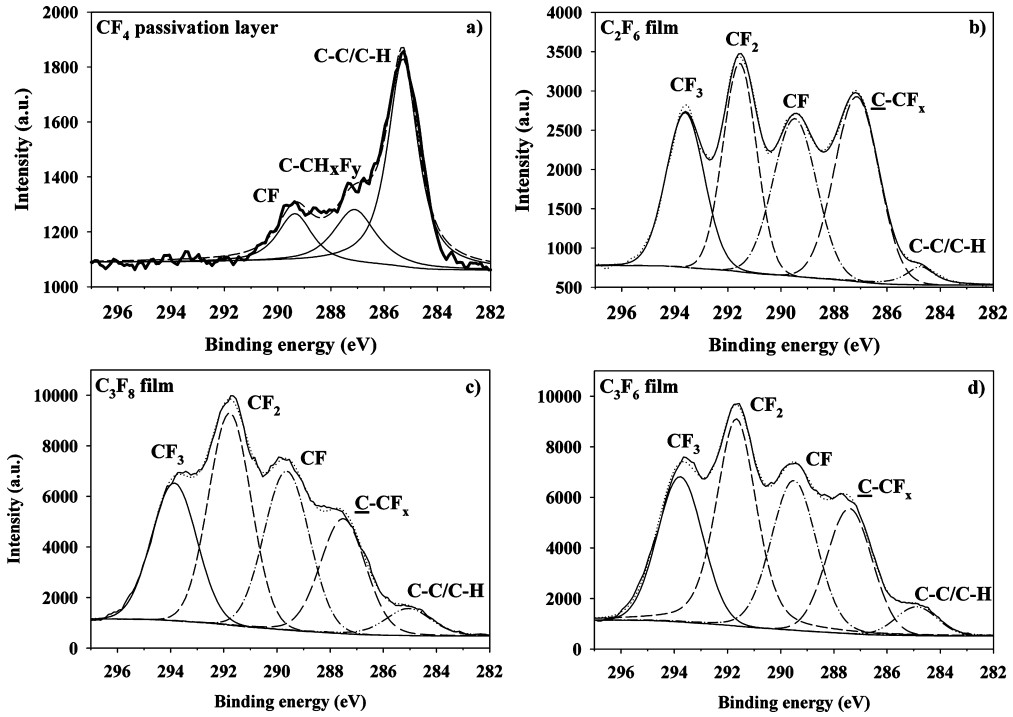

Figure 4. High-resolution C_{1s} XPS spectra for fluorocarbon films deposited from (a) CF_4, (b) C_2F_6, (c) C_3F_8, and (d) C_3F_6 plasmas. Specific binding environments are labeled accordingly.

intensities of the emission peaks were plotted as a function of t for both CF and CF_2, with Figure 1b showing a typical plot for CF_2. Clearly, the relative concentrations of both CF and CF_2 follow a first-order rate dependence, and as such, these plots were fit with a regression in the form of a three-parameter exponential decay proportional to e^{-kt}, where k represents the production rate constant for a given species. Calculated values of k for CF and CF_2 production are illustrated in panels c and d in Figure 1, respectively, as a function of P in all the C_xF_y systems studied. One important observation in both plots is that $k(CF_n)$ (where n = 1 or 2) values are very similar for CF_n production from a broad range of precursors, specifically for C_2F_6, C_3F_8, and C_3F_6 plasmas. However, CF_n production from CF_4 plasmas deviates from this trend. In particular, k(CF) values for CF_4 plasmas are similar to those for all other plasma systems at P = 50 W, but increase over these systems by a factor of four as P approaches 200 W. In contrast, $k(CF_2)$ values are consistently an order of magnitude less for CF_4 plasmas as compared to those values for all other C_xF_y systems at all P. Another notable trend in these data is that there is no strong dependence of k on P, with the sole exception of CF production from CF_4 plasmas, where again, k(CF) essentially directly correlates with increasing applied rf power.

LIF images taken during IRIS experiments are shown in images a and b in Figure 2 for CF and CF_2, respectively. In each of these schemes, the middle panels depict CF_n fluorescence from the molecular beam-only trial, whereas the left-most panels show signal from CF_n species both in the plasma beam and scattered from a Si substrate. Image subtraction yields the right image panels, which thus depict only scatter of CF_n. Cross-sections for the beam-only and scatter images are plotted as a function of distance along the laser axis in the graphs at the far right, and are used to calculate scatter coefficients. For these specific data sets, S(CF) = 0.72 and $S(CF_2)$ = 0.63 for radicals in a C_3F_6 plasma at P = 150 W. Mean S values from several different sets of images are plotted as functions of the feed gas

dx.doi.org/10.1021/am2018546 | ACS Appl. Mater. Interfaces 2012, 4, 1733–1741

y/x ratio for CF and CF_2 in panels a and b in Figure 3, respectively. These figures clearly demonstrate that P does not have as dramatic an effect on scatter values as does the choice of precursor used for the plasma. For example, $S(CF_n)$ values at a given y/x ratio generally differ by only 0.2-0.4 as a function of P. As the y/x ratio increases, a more marked disparity in scatter values appears, accentuated most dramatically by the difference in $S(CF_2)$ at P = 150 W for y/x = 4.0, where $\Delta S(CF_2)$ = 1.2, Figure 3b. Interestingly, both $S(CF)$ and $S(CF_2)$ increase with increasing y/x ratio of the C_xF_y precursor feed. As the scatter coefficient is essentially a metric of the probability for surface scatter for an individual species, an increase in $S(CF_n)$ inherently denotes a decreased propensity for reactivity at a surface. Of particular note is that the S values ultimately surpass unity, indicating a surface-mediated production mechanism for CF_n species whereby radicals are generated at a FC-passivated surface. Thus, radical-surface reactions appear to be an important and integral aspect of fluorocarbon plasma processing.

High-resolution C_{1s} XPS spectra are shown in Figure 4 for films deposited from C_xF_y precursors during IRIS experiments. Generally, with the exception of films deposited from CF_4 plasmas, the FC films appear to be amorphous, CF_2-rich, and robust, with several $-\underline{C}-F_x$ binding environments present. Generally, with decreasing y/x ratio, the FC plasmas appear to tend toward polymerizing systems that favor deposition. This agrees well with the deposition rates calculated for each of these systems, Table 3, as the duration of substrate exposure to a plasma source in a typical IRIS experiment is ~60 min. Table 3 also lists the film F/C ratio, calculated from XPS data, and the percent crosslinking (defined here as the %C−C/C−H + %$\underline{C}-CF_x$ + %CF in the high-resolution XPS spectra),[27] which demonstrate that FC film crosslinking decreases significantly as the y/x ratio of the precursor decreases. Specifically, with decreasing y/x ratios, the F/C values for the film approach 2.0, the value expected for a film composed exclusively of CF_2, and the cross-linking decreases, indicating a depletion of amorphous moieties in the film.

Table 3. Properties of Plasma-Deposited Fluorocarbon Films[a]

PECVD Source	film F/C ratio	film % cross-linking	$\Delta\gamma_c$ (dyn/cm)	deposition rate (nm/min)
CF_4	0.10(0.02)	N/A[b]	6.1(0.9)	0.12(0.02)
C_2F_6	1.0(0.1)	69(3)	23.5(0.5)	1.82(0.02)
C_3F_8	1.3(0.1)	49(2)	32.7(0.5)	3.4(0.4)
C_3F_6	1.59(0.08)	43(4)	35.2(0.7)	4.2(0.5)

[a]Values in parentheses represent one standard deviation for the measurement. [b]Percent cross-linking values were not determined for CF_4-deposited films because of the lack of CF_x binding environments in the high-resolution C_{1s} XPS spectra.

Contact angle values (θ) were used to construct Zisman plots for both deposited fluorocarbon films and bare Si substrates. Here, $\cos(\theta)$ values were plotted as a function of the surface tension of the liquid droplet used to make the CA measurement, Table 2. Figure 5 demonstrates Zisman plots for both a Si wafer analyzed prior to plasma processing, and after exposure to CF_4 plasma. These plots are fitted with a linear regression which is extrapolated to $\cos(\theta)$ = 1, where a hypothetical liquid droplet of the corresponding surface tension would be instantaneously and completely wetting. This value, denoted γ_c, is the critical surface tension,[21] and is analogous to the surface energy (γ_{sv}) of the substrate or film via the Young eq 1, where γ_{sl} represents the interfacial tension at the liquid−surface boundary.

$$\gamma_{sv} = \gamma_{lv}\cos(\theta) + \gamma_{sl} \quad (1)$$

To account for underlying substrate effects in the comparisons of surface energies, we report the value $\Delta\gamma_c$, which is the difference between the measured γ_c for a deposited FC film and the substrate (e.g., Si wafer) upon which it was deposited. Thus, the $\Delta\gamma_c$ value measured for the CF_4-deposited film illustrated in Figure 5 is 6.4 dyn/cm. Representative $\Delta\gamma_c$ values are compiled in Table 3 for all the C_xF_y-deposited films. Notably, these values generally increase with decreasing y/x ratios of the feed gas, and, more importantly, with increased fluorine content in the deposited films.

DISCUSSION

Although plasmas are widely employed for substrate processing, including etching and film deposition, the fundamental interfacial interactions that lead to surface modification are often poorly understood. Efforts to more efficiently tailor surface processing techniques require a thorough knowledge of these processes. To this end, FC systems have received much attention, with aims devoted to explicating FC plasma gas-phase species behavior and correlating this behavior with surface phenomena. The scope of investigations into these systems has expanded as FC plasmas have become more widely employed in the fabrication of such market-driven technology as integrated circuits and semiconductor devices. Here, the

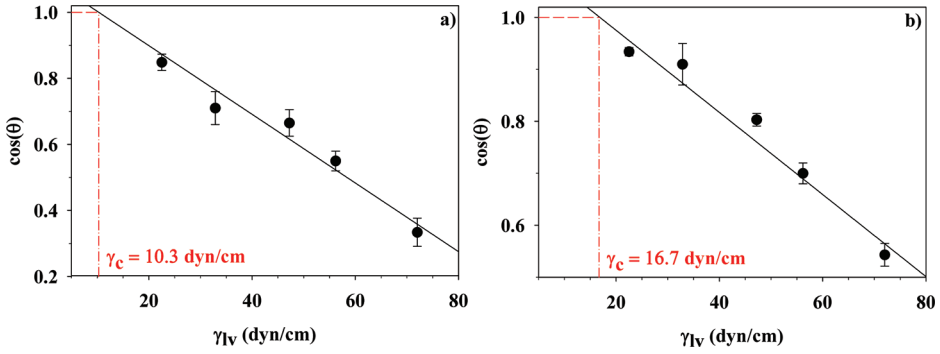

Figure 5. Zisman plots for (a) a bare Si wafer, with critical surface tension of 10.3 dyn cm^{-1} and (b) a CF_4 film deposited on Si, with γ_c = 16.7 dyn cm^{-1}. Best-fit linear regression lines are extrapolated to $\cos(\theta)$ = 1, where the value γ_c is obtained.

roles of CF_n radical species have been investigated to determine a correlation between gas-phase phenomena and film deposition from C_xF_y plasma systems.

Optical emission spectroscopy provides an expedient and practical method of gauging the behavior of gas-phase plasma species. We have examined the formation of CF* and CF_2* in the gas-phase through TR-OES. Production of these species from a given precursor follow first-order processes, whereby rate constants for production are calculated using exponential fits to the TR-OES data. These rate constants reflect the production of CF_n* species in the plasma gas-phase, but do not distinguish specific mechanisms of formation. Indeed, the complex processes that lead to generation of CF_n*, including direct decomposition of the precursor and gas-phase recombination reactions, are inherently incorporated in these k values. In addition, over a longer duration ($t \gg 0.3$ s), the apparent steady-state concentration of CF_n* species tends to decrease as consumption of the gas-phase species commences via intricate gas-phase reactions or increased dissociation of the fragment in a reactant-starved scenario. Thus, due to the complexity of the system as a whole, we focus here on the initial production of CF_n* upon plasma ignition.

The values of these rate constants are largely independent of changing P, and as such the effect of P on the efficacy of plasma production of CF_n can be ignored. The only exception to this is for k(CF) measured in CF_4 plasmas. In the CF_4 system, the linear correlation between the production rate constants and P indicates that the power applied to the system is the main driving force for CF production from the precursor. Conversely, $k(CF_2)$ in CF_4 systems is completely independent of P, such that the production rate of CF_2 is effectively constant. The value of k(CF) increases by nearly an order of magnitude over $k(CF_2)$, Figure 1c, d, demonstrating that the CF_4 system favors production of CF species over CF_2 as P increases. This appears to be unique to CF_4 plasmas in comparison to the other C_xF_y systems studied here.

CF_2 gas-phase production also appears to be dependent upon feed gas choice. The $k(CF_2)$ values measured in CF_4 plasmas are essentially an order of magnitude lower than those measured in any of the other C_xF_y systems, Figure 1d. This indicates that upon ignition of the plasma, a dearth of CF_2 units exist in CF_4 as compared to the other plasma systems. Moreover, as $k(CF_2)$ values are effectively constant for plasmas with precursor y/x ratios <4.0, we assume there is little variation in initial CF_2 concentration (i.e., t = 0–0.5 s after plasma ignition) in these plasma systems. These observations are important in that they suggest a "trickle-down" effect of a lack of CF_2 in the case of the CF_4 system. Specifically, gas-phase reactions, such as that depicted in reaction 2

$$CF_2(g) + C_mF_n(g) \rightarrow C_{m+2}F_{n+2}(g) \quad (2)$$

and suggested by Zhang and Kushner,[3] as well as other researchers,[28] generate oligomeric gas-phase species that are not necessarily formed from direct decomposition of the plasma precursor. The rate constants for such generic reactions at 50 mTorr are generally $\sim 1 \times 10^{-13}$ molecule^{-1} cm^3 s^{-1} and are expected to proceed with a third body interaction.[3,29] Indeed, Gabriel and coworkers speculated that C_2F_4 formation was the major loss mechanism of CF_2 in CF_4-based pulsed discharges.[30] These oligomeric units, in conjunction with CF_2(g) species, are thought to contribute to surface passivation and ultimately film growth at reactor walls and on substrates, reactions 3–6.

$$C_2F_4(g) + A(s) \rightarrow 2P(s) \quad (3)$$

$$C_2F_5(g) + A(s) \rightarrow 2P(s) \quad (4)$$

$$CF_2(g) + A(s) \rightarrow P(s) \quad (5)$$

$$CF_2(g) + A(s) \rightarrow 2P(s) \quad (6)$$

Interaction with an activated surface site (A(s)) can proceed to passivate the site (P(s)) and film growth can progress through continued interactions of gas-phase species with P(s), especially propagating FC films through reactions at reactive sites of passivating oligomeric units.[31] Ultimately, the languid production of CF_2 in CF_4 plasma systems may conceivably result in a significant discrepancy in FC film deposition efficacy compared to C_2F_6, C_3F_8, and C_3F_6 systems. Indeed, we observe a steep decline in deposition rate as the precursor y/x ratio approaches 4.0, Table 3. FC deposition schemes arising from film growth based upon oligomeric units (i.e., reactions 3 and 4) could be of paramount importance in C_3F_6 systems. Here, the π-bond can be easily broken under relatively mild plasma conditions to produce a highly reactive and moderately large deposition precursor.[32] Thus, C_3F_6 plasmas ought to facilitate efficient FC film initiation and propagation. Accordingly, this system demonstrates the highest deposition rate of any of the feed gases discussed here, as illustrated in Table 3.

In addition to film formation, gas-surface interactions can also promote generation of CF_n species at a fluorocarbon-passivated surface site, reactions 7 and 8. These processes illustrate the gas-phase production of CF or CF_2 via reactions involving a gas-phase oligomer. CF_n species can also interact with a surface without reacting, as in rection 9, effectively adsorbing and then desorbing intact from the surface.

$$C_mF_n(g) + P(s) \rightarrow C_{m-1}F_{n-1}(s) + CF(g) \quad (7)$$

$$C_m(g)F_n + P(s) \rightarrow C_{m-1}F_{n-2}(s) + CF_2(g) \quad (8)$$

$$CF_n(g) + A(s) \rightarrow CF_n(g) + A(s) \quad (9)$$

We have monitored the gas-surface interactions that occur in our C_xF_y systems using the imaging of radicals interacting with surfaces technique. It is apparent from these data that the choice of precursor strongly influences the propensity for CF_n surface scatter, as both S(CF) and $S(CF_2)$ increase with increased feed gas y/x ratio, Figure 3. In particular, S values far surpass unity as the precursor y/x ratio approaches 4.0, indicating a significant increase in the amount of CF_n(g) produced at surfaces during deposition of FC films.

The dependence of S on precursor choice can be rationalized in a number of ways. Specifically, in the highly depositing systems (those with low y/x ratios; C_3F_6 and C_3F_8), a wealth of reactive species, including oligomers with unpaired electrons, exist in the gas phase. These include a plethora of C_2F_4, C_2F_5, C_3F_5, and C_3F_3, as verified in our systems by mass spectrometric analyses. Under conditions in which such gas-phase species proliferate, as in the case of low y/x ratio precursors, recombination with surface-produced CF_n and subsequent redeposition of the product is plausible. Such a scenario effectively reduces the observed scatter coefficient for CF_n species by consuming CF_n produced via reactions 7–9.

In these scenarios, one must consider the effect of ions as well. Average ion energy $\langle E_i \rangle$ values in our systems increase

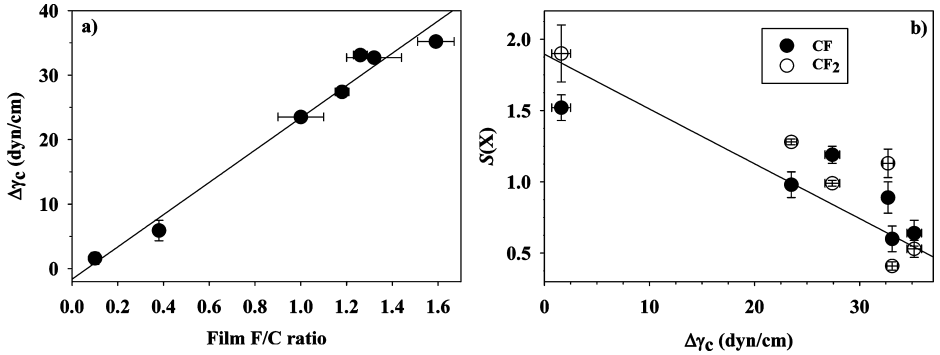

Figure 6. (a) $\Delta\gamma_c$ values plotted as a function of film fluorine to carbon ratios (obtained from XPS analyses) fitted with a linear regression where R^2 = 0.98. (b) Scatter coefficients, S(CF) and $S(CF_2)$, plotted as a function of $\Delta\gamma_c$, with a linear fit with R^2 = 0.80.

significantly with increasing y/x ratio of the precursor, such that the total average ion energies in the CF_4 plasma system are approximately twice those of the C_3F_6 system. We have previously demonstrated that ion bombardment can be a major contributing factor in surface production of CF_2, and that $\langle E_i \rangle$ and S values correlate linearly.[16,33] Thus, ions may be partially responsible for the rise seen in S as the plasma precursor y/x ratio increases. A third contributing factor to consider is the relative distribution of electronically excited CF_n states in the plasma gas-phase. Because our IRIS experiments probe only ground state CF or CF_2 radicals, excited species are disregarded. Especially with CF surface interactions, however, the electronic excited states appear to have a strong influence on the observed S(CF) value. Using OES, we generally observe increasing relative concentrations of excited $CF(^2\Delta)$ with increasing precursor y/x ratios, concomitant with significantly increased vibrational temperatures. We speculate that the $CF(^2\Delta)$ quenches upon interaction with the surface. Unfortunately, this excited state is inaccessible using our current IRIS apparatus due to wavelength limitations. The increased vibrational energy associated with the molecule assists it in overcoming a barrier of desorption to re-enter the gas-phase as a ground state $CF(^2\Pi)$ radical, detectable in our LIF scheme. This particular scenario is exacerbated as the plasma precursor y/x ratio increases, making it a potential contribution to the increase in observed S(CF).

The net effect of gas-surface interactions can be gauged by analyzing the deposited FC film. It is clear from high-resolution C_{1s} XPS analyses of substrates processed in IRIS experiments that CF_4 plasmas generally do not deposit a robust FC film as compared to the other C_xF_y systems. Note that the difference in substrate processing times among different C_xF_y precursors in IRIS experiments was negligible, such that the duration of plasma exposure corresponding to each spectrum in Figure 4 was essentially identical. Thus, the disparity in CF_4 film deposition is thought to result from a combination of the lack of formation of film-forming or film-propagating units in the gas-phase of the CF_4 system and the effect of ion bombardment on passivating FC films. These data complement the idea that CF_4 plasmas are generally considered highly proficient etching systems. As the y/x ratio of the plasma system decreases from 4.0, the FC films tend to become less crosslinked and the films' fluorine content increases, indicating a higher degree of incorporation of CF_2 species (Table 3). These increases in film fluorine content are concomitant with increases in film surface energy, $\Delta\gamma_c$. Notably, this correlation is linear, Figure 6a, where $\Delta\gamma_c$ values are plotted as a function of the corresponding film F/C ratio. These data were collected for films deposited in independent plasma reactors, not in the IRIS apparatus, at a range of plasma conditions, and include data for each of the C_xF_y precursors. Although this relationship would seem to imply that the surface energy is dependent upon the potential of interaction and that increasing fluorine content increases the film potential, this is not the case. Indeed, Zisman was among the first to report there is effectively no difference in potential of interaction of $C-F_x$ and $C-H_x$ species in contact angle experiments.[21] Thus, the relationship between fluorine content and surface energy is related to the packing efficiency of propagating units in the FC film.[21,34] Specifically, the contact angle of a liquid droplet is dependent upon the molar volume of C-X (where X = C, H, or F) with which it comes in contact. Zisman suggests that surfaces rich in $-CF_n-$ linkages are likely to give rise to high surface energies.[21] As such, the move toward higher $\Delta\gamma_c$ and increased fluorine content in the film could indicate a greater extent of surface coverage of CF_n moieties.

Although the $\Delta\gamma_c$ values reported here tend to be higher than many values reported in the literature for FC films,[35,36] we expect the general trends observed here to be valid. One possible contributing factor to the apparently high surface energy values measured herein may lie in the method used for investigation. The variability in contact angles with decreasing surface tension of the contact droplet (i.e., higher relative concentration of methanol to water) becomes much more significant as the droplet more completely wets the FC film and results are generally skewed toward higher CA values. As such, the extrapolated fits to CA data yield results of a higher surface energy. Despite these potential sources of bias, the overall shift toward higher surface energy with increased CF_2 content in the FC film is reasonable.

Generally, FC films deposited on Si wafers tend to be smooth and relatively defect-free, as confirmed by SEM and AFM analyses. It is of interest, however, to gauge whether the phenomena associated with $\Delta\gamma_c$ is dependent upon surface roughness. To this end, C_3F_6 films were deposited on supported Fe_2O_3 nanoparticle surfaces.[37] Values for rms roughness were calculated for 2500 μm^2 areas on both FC-coated and uncoated Fe_2O_3 substrates. The deposition of a FC film on Fe_2O_3 nanoparticles (rms roughness = 0.84 ± 0.05 μm) resulted in a slight decrease in surface roughness over uncoated particles (rms roughness = 1.05 ± 0.09 μm). These roughness factors are nevertheless significantly higher than the rms roughness of a FC film on a flat Si substrate, ~0.01 μm. Despite these differences in roughness, the morphology of the surface appears to have little influence over the calculated value of $\Delta\gamma_c$.

dx.doi.org/10.1021/am2018546 | ACS Appl. Mater. Interfaces 2012, 4, 1733−1741

Specifically, the surface energy of a C_3F_6-deposited film on Fe_2O_3 nanoparticles was calculated as 31.9 ± 0.6 dyn/cm, compared to 35.9 ± 0.5 dyn/cm for the same type of FC film on a Si substrate.

The surface energies of deposited FC films have also been related to observed scatter coefficients for CF and CF_2, as shown in Figure 6b. Here, the indirect relationship between S and $\Delta\gamma_c$ suggests there exists a net balance between the processes that drive these two measures. On one hand, a low $\Delta\gamma_c$ and high scatter coefficient could indicate a loss of surface $-CF_n-$ via those processes which induce large surface scatter, as discussed above. Alternatively, a dearth of scatter-inducing processes where S is low may render the film relatively unaffected, resulting in a larger $\Delta\gamma_c$ due to a larger surface concentration of $-CF_n-$. The dichotomous nature of this relationship, whether $\Delta\gamma_c$ increases because S decreases, or vice versa, is a point of ongoing consideration in our laboratory. Ultimately, the ability to tailor surface properties of deposited films via choice of plasma precursor promises to impact a wide range of applications. Some examples include the reduction of membrane fouling by membrane modification to low surface energy[38] or modification to high-surface-energy materials for use in biologically compatible implants.[39]

SUMMARY

Appropriate precursor selection is a critical element for further advancement of applications employing plasma-deposited fluorocarbon films. As demonstrated here, efficacy of film deposition is strongly dependent on the C_xF_y source, stemming largely from gas-phase phenomena which drive the formation of depositing units. Specifically, recombination reactions that generate oligomeric deposition precursors are significantly limited in C_xF_y with $y/x > 3$. The behavior of species at the depositing interface appears to dictate the resulting surface characteristics of deposited FC films, especially the surface energy. Moreover, the y/x ratio of the precursor directly affects the amount of fluorine incorporation in a deposited film, and film fluorine content, in turn, influences the arrangement of $-CF_n-$ moieties at the surface. The combination of gas-phase diagnostics such as TR-OES, gas-surface interface data obtained via our IRIS technique, and surface analyses including XPS and contact angle measurements provide significant insight into the molecular-level mechanisms at the core of film deposition in fluorocarbon plasmas. The ability to carefully select the appropriate plasma precursor, in addition to other plasma parameters, provides the ability to tailor the surface properties of a deposited film, thereby creating specific high-performance materials for a range of applications.

AUTHOR INFORMATION

Corresponding Author

*E-mail: ellen.fisher@colostate.edu.

Notes

The authors declare no competing financial interest.

ACKNOWLEDGMENTS

This work was supported by the National Science Foundation (CHE-0911248). M.F.C. also acknowledges financial support from the Department of Defense Science, Mathematics, and Research for Transformation (SMART) fellowship.

REFERENCES

(1) Ludvik, M.; Daniel, P. *J. Vac. Sci. Technol. A* **2000**, *18*, 2619−2645.
(2) Jin, Y.; Ajmera, P.; Lee, G.; Singh, V. *J. Electron. Mater.* **2005**, *34*, 1193−1205.
(3) Feng, L.; Li, S.; Li, Y.; Li, H.; Zhang, L.; Zhai, J.; Song, Y.; Liu, B.; Jiang, L.; Zhu, D. *Adv. Mater.* **2002**, *14*, 1857−1860.
(4) Haïdopoulos, M.; Turgeon, S.; Laroche, G.; Mantovani, D. *Plasma Process. Polym.* **2005**, *2*, 424−440.
(5) Nelea, V.; Holvoet, S.; Turgeon, S.; Mantovani, D. *J. Phys. D: Appl. Phys.* **2009**, *42*, 225208.
(6) Lewis, F.; Cloutier, M.; Chevallier, P.; Turgeon, S.; Pireaux, J.-J.; Tatoulian, M.; Mantovani, D. *ACS Appl. Mater. Interfaces* **2011**, *3*, 2323−2331.
(7) Lewis, F.; Horny, P.; Hale, P.; Turgeon, S.; Tatoulian, M.; Mantovani, D. *J. Phys. D: Appl. Phys.* **2008**, *41*, 045310.
(8) Shuwu, W.; Gupta, A. S.; Sagnella, S.; Barendt, P. M.; Kottke-Marchant, K.; Marchant, R. E. *J. Biomater. Sci., Polym. Ed.* **2009**, *20*, 619−635.
(9) Smith, B. K.; Sniegowski, J. J.; LaVigne, G.; Brown, C. *Sens. Actuators, A: Phys.* **1998**, *70*, 159−163.
(10) Wiedemair, J.; Balu, B.; Moon, J.-S.; Hess, D. W.; Mizaikoff, B.; Kranz, C. *Anal. Chem.* **2008**, *80*, 5260−5265.
(11) d'Agostino, R.; Cramarossa, F.; Fracassi, F. *Plasma Deposition, Treatment, and Etching of Fluorocarbons*; Academic Press: San Diego, CA, 1990.
(12) Biederman, H. *Plasma Polymer Films*; Imperial College Press: London, 2004.
(13) Haverlag, M.; Stoffels, E.; Stoffels, W. W.; Kroesen, G. M. W.; Hoog, F. J. d. *J. Vac. Sci. Technol. A* **1994**, *12*, 3102−3108.
(14) Milella, A.; Palumbo, F.; Favia, P.; Cicala, G.; d'Agostino, R. *Plasma Process. Polym.* **2004**, *1*, 164−170.
(15) Butoi, C. I.; Mackie, N. M.; Williams, K. L.; Capps, N. E.; Fisher, E. R. *J. Vac. Sci. Technol., A* **2000**, *18*, 2685−2698.
(16) Cuddy, M. F.; Fisher, E. R. *J. Appl. Phys.* **2010**, *108*, 033303.
(17) Butoi, C. I.; Mackie, N. M.; Barnd, J. L.; Fisher, E. R.; Gamble, L. J.; Castner, D. G. *Chem. Mater.* **1999**, *11*, 862−864.
(18) Butoi, C. I.; Mackie, N. M.; Gamble, L. J.; Castner, D. G.; Barnd, J.; Miller, A. M.; Fisher, E. R. *Chem. Mater.* **2000**, *12*, 2014−2024.
(19) Owens, D. K.; Wendt, R. C. *J. Appl. Polym. Sci.* **1969**, *13*, 1741−1747.
(20) Johnson, K. L.; Kendall, K.; Roberts, A. D. *Proc. R. Soc. Chem., Ser. A−Math. Phys.* **1971**, *324*, 301−313.
(21) Fox, H. W.; Zisman, W. A. *J. Colloid Sci.* **1950**, *5*, 514−531.
(22) McCurdy, P. R.; Bogart, K. H. A.; Dalleska, N. F.; Fisher, E. R. *Rev. Sci. Instrum.* **1997**, *68*, 1684−1693.
(23) Mackie, N. M.; Dalleska, N. F.; Castner, D. G.; Fisher, E. R. *Chem. Mater.* **1997**, *9*, 349−362.
(24) Mackie, N. M.; Castner, D. G.; Fisher, E. R. *Langmuir* **1998**, *14*, 1227−1235.
(25) Booth, J. P.; Cunge, G.; Chabert, P.; Sadeghi, N. *J. Appl. Phys.* **1999**, *85*, 3097.
(26) Stillahn, J.; Trevino, K.; Fisher, E. R. *Annu. Rev. Anal. Chem.* **2008**, *1*, 261−91.
(27) Luginbuhl, R.; Garrison, M. D.; Overney, R. M.; Weiss, L.; Schieferdecker, H.; Hild, S.; Ratner, B. D. *Fluorinated Surfaces, Coatings, and Films*; American Chemical Society: Washington, D.C., 2001.
(28) Stoffels, E.; Stoffels, W. W.; Tachibana, K. *Rev. Sci. Instrum.* **1998**, *69*, 116−122.
(29) Plumb, I. C.; Ryan, K. R. *Plasma Chem. Plasma Process.* **1986**, *6*, 205−230.
(30) Gabriel, O.; Stepanov, S.; Meichsner, J. *J. Phys. D: Appl. Phys.* **2007**, *40*, 7383.
(31) Cunge, G.; Booth, J. P. *J. Appl. Phys.* **1999**, *85*, 3952−3959.
(32) Leezenberg, P. B.; Reiley, T. C.; Tyndall, G. W. *J. Vac. Sci. Technol., A* **1999**, *17*, 275−281.
(33) Martin, I. T.; Zhou, J.; Fisher, E. R. *J. Appl. Phys.* **2006**, *100*, 013301.

(34) Hoernschemeyer, D. *J. Phys. Chem.* **1966**, *70*, 2628−2633.
(35) Zhuang, Y. X.; Menon, A. *J. Vac. Sci. Technol., A* **2005**, *23*, 434−439.
(36) Scholberg, H. M.; Guenthner, R. A.; Coon, R. I. *J. Phys. Chem.* **1953**, *57*, 923−925.
(37) Shearer, J. C.; Fisher, E. R. *Nanosci. Nanotechnol. Lett.*, **2012**, accepted.
(38) Hamza, A.; Pham, V. A.; Matsuura, T.; Santerre, J. P. *J. Membr. Sci.* **1997**, *131*, 217−227.
(39) Baier, R. E. *Bull. NY Acad. Med.* **1972**, *48*, 257−272.
(40) Vazquez, G.; Alvarez, E.; Navaza, J. M. *J. Chem. Eng. Data* **1995**, *40*, 611−614.